An individual-based simulation framework for dynamic, heterogeneous cell populations during extrinsic stimulations

Dirke Imig[1], Nadine Pollak[2], Timm Strecker[1], Peter Scheurich[2], Frank Allgöwer[1], and Steffen Waldherr[3] *

[1]*Institute for Systems Theory and Automatic Control, University of Stuttgart, Pfaffenwaldring 9, 70550 Stuttgart, Germany*
[2]*Institute of Cell Biology and Immunology, University of Stuttgart, Allmandring 31 , 70569 Stuttgart, Germany and*
[3]*Institute for Automation Engineering, Otto von Guericke University Magdeburg, Universitätsplatz 2, 39106 Magdeburg, Germany*

(Dated: December 11, 2015)

As experimental measurements consider cell populations rather than individual cells and because of the awarness of the role of heterogeneity in cellular systems, mathematical modeling of populations became a systems biological focus in recent years. When investigating the response behavior of cells to extrinsic stimulations, processes on the level of the population such as directional selection and inheritance must be taken into account. In this work, an individual-based modeling framework for the efficient analysis and simulation of heterogeneous cell populations is presented. With help of prior knowledge about stationary population characteristics, initial conditions of model states and parameters are derived. As cell division, cell death and inheritance are considered realistically, short-term as well as long-term responses of cell populations can be analyzed and predicted. The model provides information about population dynamics and, furthermore, about states in individual cells, also with respect to different cell cycle phases. The framework is applied to the biologically relevant scenarios of ligand-induced apoptosis and cell differentiation. Within short simulation times, a representative number of cells can be simulated so that a comprehensive analysis of the model is possible. For future applications, other single cell models of interest can easily be included into the population framework, allowing the investigation of effects caused by cell heterogeneity.

Keywords: Heterogeneous Cell Populations, Cell Ensemble Modeling, Individual-based Modeling, Cell-to-Cell Variability, Dynamical Systems.

1. INTRODUCTION

Complex data sets obtained in cell-biological experiments include information about protein distributions through flow cytometry experiments, mean protein quantities measured via Western blots, and reaction rates estimated with help of biosensors [1, 36, 39]. In order to understand biological processes, experimentally gained information, published data and hypotheses should be considered altogether. For this purpose, appropriate mathematical models are necessary.
With help of single cell models, cell-intrinsic mechanisms can be investigated: A detailed description of molecular pathways is chosen but effects of the dynamical behavior on the level of the population are neglected. For a holistic understanding of processes, looking at a single average cell is often not sufficient. It became clear in recent years, that heterogeneity of cells in a population is important to consider [25]. Dynamics of the population can be described for example by partial differential equations (PDEs) [3, 31]. A drawback of this model class is a limited level of detail in the description of molecular mechanisms. Stochastic differential equation (SDE) models [17] or models based on the cell population master equation [37] exhibit a higher level of detail but are difficult in handling. The main challenge referring to modeling of cell populations is to find the right balance between a sufficient degree of detail for the given problem and adequate simulation runtimes for analysis. In this work, the following three goals are aimed: a) Sufficiently detailed in description of signaling pathways to analyze molecular mechanisms, b) appropriate description of cell population dynamics and c) reasonable handling and simulation time. On this basis, we chose a cell ensemble approach where a representative large number of individual cells that forms a cell population is parametrized and simulated. Although the first ensemble-based approach was already published in 1984 by Domach and Shuler [10], only a small number of comprehensive models were developed in the meantime. The main drawback of the method is the computational power that is needed for simulation of a sufficiently large number of cells. Therefore, most of the published individual-based models neglect the event of cell division [14, 19, 32, 33] and are therefore only valid for a short time period. Due to enhanced computer efficiency, simulations of larger models are facilitated and development of extensive individual-based models will become a stronger focus in the next years. Ensemble models including cell division can be found for example in Volfson et al. [42] and Bertaux et al. [7]. We included cell division and cell death in dependence on intracellular states which can be regarded as extension of the idea presented by Mantzaris [26] where cell division was modeled dependently on a single state. Our model allows an efficient

*Corresponding author. Email: steffen.waldherr@ovgu.de, Tel.: +49 391 67 58948.

analysis of state trajectories in individual cells over long timescales. Volfson et al. [42] only differentiate between two generations, mother and daughter cells. In contrast to Bertaux et al. [7], the description of gene expression is replaced in our approach by introducing different synthesis rates, and a simplified description of inheritance from mother to daughter cells is chosen where each cell inherits parameters within given borders. New in our framework is also to systematically split the model into different levels, where parameters are sampled subsequent cell division on the level of the population. After cell division, ordinary differential equations are solved deterministically for each cell, not stochastically as described in Bertaux et al. [7]. Hence, the efficiency of established ODE solvers can be exploited. Furthermore, volume growth is included in our model and different cell cycle phases can be distinguished. Relevant data for model initialization involve average protein amounts in cell populations, and also flow cytometry data revealing information referring to properties of protein distributions. Model simulations can be compared and adapted to data of cell numbers and protein amounts over time. Irreversible changes within cell populations are not taken into account. Therefore, the time frame of model simulation is limited to scenarios where mutations are negligible. Direct cell-to-cell communication of cells and morphological influences are also neglected. Nevertheless, the presented population model is sufficient for investigation of several biological scenarios.

Chapter 2 focuses on the description of different model levels. Initial conditions are derived with help of minimal models and the simulation algorithm is outlined. The application of the modeling framework to two biological examples is presented in Chapter 3: Ligand-induced apoptotic response on basis of the model described in Eissing et al. [11], and a model of cell differentiation developed by Schittler et al. [30] are put into the proposed population modeling framework, simulated and analyzed.

2. MODELING OF CELL POPULATION DYNAMICS

In this chapter, a compact mathematical description of the developed model is given. The model can be divided into three levels (Figure 1). On the first level, a cellular process of interest is described via ordinary differential equations (ODEs). The second level considers the diversity of cells in a population. In Section 2 2.2 the stationary heterogeneity of cells in a population before exposure to a stimulation is investigated. The third level concerns the population dynamics. In the following, the different model features are elucidated in detail.

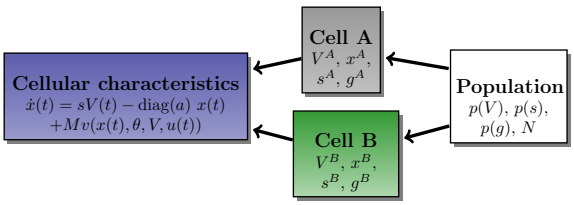

FIG. 1: **Model overview.** The model consists of three levels: cellular characteristics, heterogeneous cells and the population level. Cellular characteristics involve the dynamics of states x in each cell. Individual cells differ in volume V, growth rate g, synthesis rates s and states x. The number N of simulated cells in a population depends on cell division and cell death. Volumes, synthesis rates and growth rates are initially sampled from predefined distributions $p(V), p(g), p(s)$.

2.1. Cellular characteristics

A system of ODEs describing the intracellular process of interest is the basis of the model. States represent for example amounts of proteins but also other molecules can be considered. The dynamical behavior of the states $x \in \mathbb{R}^n$ in one cell is described in the form of

$$\begin{aligned} \dot{x}^i(t) =& s^i V^i(t) - \mathrm{diag}(a)\ x^i(t) \\ &+ Mv(x^i(t), \theta, V^i(t), u(t)), \end{aligned} \tag{1}$$

$$i \in [1, ..., N],$$

where i is the index for the i-th cell in a population of N cells. $M \in \mathbb{R}^{n \times m}$ represents the stoichiometric matrix containing information about the interactions of states within each single cell. Because of genetic identity of a clonal cell population, the main cellular characteristics described in M are assumed to be structurally the same in all cells, similar as described in Hasenauer et al. [18] and Waldherr et al. [43]. Parameters in vector $\theta \in \mathbb{R}^w$ are for example kinetic reaction rate constants and binding affinities. Degradation and synthesis rates of proteins are considered in $a \in \mathbb{R}^n$ and $s^i \in \mathbb{R}^n$ respectively. The time-dependent cell volume $V^i \in \mathbb{R}$ is considered in the reaction rate vector $v \in \mathbb{R}^m$ and in the synthesis of proteins. So far, production of proteins depends linearly on the volume. When corresponding data are available, further dependencies could be considered. $u(t) \in \mathbb{R}$ is the time-dependent system stimulus.

2.2. Stationary heterogeneity of cells: Volume distribution, initial conditions and protein synthesis

The dynamics of a cell population is deduced by simulating a certain number of cells, while each cell contains the same ODE network introduced above. Although cells in a clonal population usually have the same genetic make-up, they differ in cell cycle stages and gene expression rates, the latter presumably building the main factor for cell heterogeneity [27, 33, 35]. For simplification, gene expression is represented by synthesis of proteins in the model. Hence,

selected production rates s_h are heterogeneously distributed in the population. Values of synthesis rates can be estimated according to underlying data and information (see Equation (26)). The vector of synthesis rates is given by

$$s^i = \begin{pmatrix} s_h^i \\ s_c \end{pmatrix}, \tag{2}$$

where the vector s_c denotes synthesis rates which take the same value for all cells. Different phases in the cell cycle, the other important source of heterogeneity in an asynchronous population, are represented in the model by different cell volumes (see Equation (18)). Experimental distinction between linear or exponential growth of the cell size is difficult and publications supporting both theories exist [8, 9, 23, 41]. As the detailed investigation of cell size characteristics is not the focus of this work, the simplifying assumption of cell size-independent cell growth is chosen. In the model, the cell volume evolves linearly according to the ODE

$$\dot{V}^i(t) = g^i(x^i(t)) \tag{3}$$

with initial condition

$$V^i(0) = V_0^i$$

on the single cell level with a growth rate $g^i(x^i(t)) \geq 0$. In some systems, the growth rate may be independent of the considered cellular states. It is then simply sampled from a probability distribution with density function $p(g)$,

$$g^i \sim p(g). \tag{4}$$

Biological observations indicate that a normal distribution is a good model for the heterogeneity in the growth rate [22]. The initial condition for the distribution of cellular volumes $V^i(0)$ in the population is derived from the time-invariant solution of a simple cell population balance model. For simplicity, this derivation assumes that the only heterogeneous variable is the cell volume V, evolving linearly, and that the growth rate $g^i = g$ is the same for all cells. The dynamics of the cell population are then described by the PDE

$$\frac{\partial p}{\partial t} + g\frac{\partial p}{\partial V} = 0\,, \tag{5}$$

where $p(t, V)$ is the cell density. Equation (5) is defined on the domain $[\frac{V_d}{2}, V_d]$, where V_d represents the division volume that is halved after division (see Section 2 2.3). Hence, the system has the boundary condition

$$p(t, \frac{V_d}{2}) = 2p(t, V_d)\,. \tag{6}$$

The relative density function $\overline{p}(t, V)$ is defined by $p = N\overline{p}$, where N is the cell number described by

$$N(t) = \int_{\frac{V_d}{2}}^{V_d} p(t, V)dV\,, \tag{7}$$

leading to

$$\int_{\frac{V_d}{2}}^{V_d} \overline{p}(t, V)dV = 1\,. \tag{8}$$

The relative density evolves according to the PDE

$$\dot{N}\overline{p} + N\frac{\partial \overline{p}}{\partial t} + Ng\frac{\partial \overline{p}}{\partial V} = 0\,. \tag{9}$$

From (5) and (6), the time derivative of the cell number is then

$$\begin{aligned}\dot{N}(t) &= \int_{\frac{V_d}{2}}^{V_d} \frac{\partial p}{\partial t}dV = -\int_{\frac{V_d}{2}}^{V_d} g\frac{\partial p}{\partial V}dV \\ &= gp(t, \frac{V_d}{2}) - gp(t, V_d) = g\overline{p}(t, V_d)N(t)\,.\end{aligned} \tag{10}$$

In the following, we denote

$$k(t) = g\overline{p}(t, V_d)\,. \tag{11}$$

Substituting $\dot{N}$ from (10) in (9), we get

$$Nk(t)\overline{p} + N\frac{\partial \overline{p}}{\partial t} + Ng\frac{\partial \overline{p}}{\partial V} = 0\,. \tag{12}$$

It follows that

$$k(t)\overline{p} + \frac{\partial \overline{p}}{\partial t} + g\frac{\partial \overline{p}}{\partial V} = 0\,. \tag{13}$$

Let $\overline{p}_s(V)$ be a time-invariant solution, and

$$k_s = g\overline{p}_s(V_d)\,. \tag{14}$$

The time-invariant solution needs to satisfy the equation

$$k_s\overline{p}_s + g\frac{\partial \overline{p}_s}{\partial V} = 0\,. \tag{15}$$

Solving for $\overline{p}_s$, we obtain

$$\overline{p}_s(V) = \frac{k_s}{g}e^{\frac{k_s}{g}(V_d - V)}\,, \tag{16}$$

where the end-point condition (14) has already been taken into account. From the integral condition (8), we find

$$-e^{\frac{k_s}{g}(V_d - V)}\Big|_{\frac{V_d}{2}}^{V_d} = e^{\frac{k_s V_d}{2g}} - 1 = 1 \tag{17}$$

and thus $k_s = \frac{2g\ln 2}{V_d}$. The time-invariant relative density function of the cell volume is thus given by

$$\overline{p}_s(V) = \frac{2\ln 2}{V_d}e^{2\ln 2(1 - \frac{V}{V_d})}\,. \tag{18}$$

Hence, the balance equation (5) has a time-invariant solution $\bar{p}_s(V)$ for the relative volume density (Figure 2) that is independent on the growth rate g and is of exponential

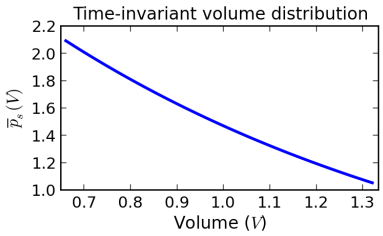

FIG. 2: **Volume distribution.** The relative time-invariant volume distribution is exponentially distributed.

shape. With the linear growth model, cell volume is proportional to cell age, and an exponential cell age distribution has been proposed in earlier research [10]. However, the mathematical derivation based on a population balance model done here seems to be novel. The overall population model is initialized from a volume distribution with density $p(V_0) = N_0 \bar{p}_s(V_0)$.

Next, we discuss the stationary heterogeneity in the protein synthesis rates s. Experimentally obtained information usually contains flow cytometry-derived data representing protein distributions $p(X)$ in an untreated cell population. While no external changes occur, the distributions of protein numbers are time-invariant in a population. A measurement of the synthesis rate distribution $p(s)$ can be very complicated or is often not even possible. Considering measurements of the degradation rate a, the equilibrium distribution $p(X)$, and estimating the growth rate probability distribution $p(g)$, the distribution of synthesis rate $p(s)$ can be calculated. In our model formulation, interactions between components of the signaling pathway are non-existing while the system's input is zero, leading to the following simplification of Equation (1) that is valid during the life span of a cell (here considered to be the interval $[0,\, t_{cyc}]$) for every protein $x_z, z \in [1, ..., n]$ in each single cell:

$$\dot{x}_z^i(t) = s_z^i V^i(t) - a_z x_z^i(t)\ , \tag{19}$$

$$x_z^i(0) = x_{z,0}^i,$$

$$V^i(0) = \frac{V_d}{2},$$

where $\frac{V_d}{2}$ represents the cell volume at the beginning of the cell cycle, subsequent to cell division (see Section 2 2.3). Considering linear cell growth (Equation (3)), the equation can be solved for $x_z^i(t)$.

$$x_z^i(t) = e^{-a_z t} x_{z,0}^i + \int_0^t (s_z^i \frac{V_d}{2} + s_z^i g^i \tau) e^{a_z(\tau - t)} d\tau \tag{20}$$

$$\begin{aligned} x_z^i(t) = e^{-a_z t} x_{z,0}^i + \frac{s_z^i (g^i (a_z t - 1) + a_z \frac{V_d}{2})}{{a_z}^2} \\ - \frac{s_z^i e^{-a_z t} (-g^i + a_z \frac{V_d}{2})}{{a_z}^2}\ , \end{aligned} \tag{21}$$

where s_z^i, a_z and g^i are constant during one cell cycle. The duration of the cell cycle can be calculated by

$$t_{cyc}^i = \frac{V_d}{2 g^i}\ . \tag{22}$$

In order to approximate biologically reasonable distribution of synthesis rates, it is assumed in the following calculations that the number of each molecule is doubled during the time of one cell cycle. This leads to

$$\begin{aligned} 2x_{z,0}^i =& e^{-a_z t_{cyc}^i} x_{z,0}^i + \frac{s_z^i (g^i (a_z t_{cyc}^i - 1) + a_z \frac{V_d}{2})}{{a_z}^2} \\ & - \frac{s_z^i e^{-a_z t_{cyc}^i} (-g^i + a_z \frac{V_d}{2})}{{a_z}^2}\ . \end{aligned} \tag{23}$$

Hence, $x_{z,0}^i$ can be described as

$$\begin{aligned} & x_{z,0}^i = \\ & s_z^i \frac{(g^i (a_z t_{cyc}^i - 1) + a_z \frac{V_d}{2}) - e^{-a_z t_{cyc}^i} (-g^i + a_z \frac{V_d}{2})}{(2 - e^{-a_z t_{cyc}^i}) {a_z}^2} \end{aligned} \tag{24}$$

In the next step, the exponential volume distribution of cells (Equation (18)) is added. In order to describe the cell population, $\mathbf{X}_z$, $\mathbf{V}$ and $\mathbf{G}$ are introduced as random variables with distributions given by the density functions $p(X_z)$, $\bar{p}_s(V)$ and $p(g)$. Through the independent random variables $\mathbf{V}$ and $\mathbf{G}$ the related $\mathbf{T}$ can be deduced.

$$\mathbf{T} = \frac{\mathbf{V} - \frac{V_d}{2}}{\mathbf{G}}\ . \tag{25}$$

Inserting $t = \mathbf{T}$ and $x_{z,0}^i$ (Equation (24)) in Equation (21), the relation between $\mathbf{X}_z$, $\mathbf{G}$ and the unknown random variable $\mathbf{s}_z$ can be calculated.

$$\mathbf{X}_z = \mathbf{s}_z\ \mathbf{k}(\mathbf{V}, \mathbf{G}, a_z, V_d) \tag{26}$$

with

$$\begin{aligned} & \mathbf{k}(\mathbf{V}, \mathbf{G}, a_z, V_d) = \\ & e^{-a_z \mathbf{T}} \frac{(\mathbf{G}(a_z \mathbf{t_{cyc}} - 1) + a_z \frac{V_d}{2}) - e^{-a_z \mathbf{t_{cyc}}} (-\mathbf{G} + a_z \frac{V_d}{2})}{(2 - e^{-a_z \mathbf{t_{cyc}}}) {a_z}^2} \\ & + \frac{(\mathbf{G}(a_z \mathbf{T} - 1) + a_z \frac{V_d}{2}) - (e^{-a_z \mathbf{T}} (-\mathbf{G} + a_z \frac{V_d}{2}))}{{a_z}^2}\ . \end{aligned} \tag{27}$$

With representative samples of $\mathbf{V}$ and $\mathbf{G}$, the probability density $p(k)$ is estimated by kernel density estimator. $p(s)$ can be computed by taking the logarithm in Equation (26) and calculating $p(\log(s))$ as the deconvolution of $p(\log(X))$ and $p(\log(k))$. Mathematica and Matlab are used for analysis.

When further information about covariances of protein copy numbers and cell volumes are available, the information can be included by sampling from an appropriate multivariate joint distribution (see Kallenberger et al. [20]).

2.3. Cell death, division, and inheritance

During the population simulation, the ODE (1) for the intracellular process is solved until the end of the cell's life-cycle, which is due to either cell death or cell division.

In the modeling framework, cell death can be triggered independently from the intracellular process, for example by sampling from a population-specific distribution of expected cellular life times, or it can be triggered from the intracellular process when a certain condition on the state variable $x^i(t)$ is met. The latter option requires the use of an ODE solver which can detect threshold passing, for example the CVODE routine with root finding from the SUNDIALS library (`http://computation.llnl.gov/casc/sundials/main.html`). In the simulation, the corresponding cell is removed from the active population upon a death event.

Cell division is triggered when volume V^i, evolving according to (3), reaches the division volume V_d. In case of a constant growth rate g^i, the division time can be computed *a priori* for each cell from the analytical solution to the volume ODE (3). Otherwise, when the growth rate depends on the state $x^i(t)$ of the intracellular process, the volume ODE has to be solved together with the intracellular process' ODE (1), and a division event is triggered when $V^i(t) = V_d$. As in the cell death case, the latter option requires the use of a suitable ODE solver.

Upon division, both arising daughter cells obtain a new value of the growth rate via $p(g)$. The volume of both cells is set to $V^i(t) = V_d/2$, similar as described in Swain et al. [38]. Furthermore, new values of synthesis rates s_h of both created cells i_a and i_b are calculated within given borders. Here, a new, restricted sample of $p(s_z)$ is drawn where the value of $\mathbf{s}_z$ cannot exceed a certain multiple of the corresponding sample of the mother cell (Figure 3), so that

$$\mathbf{s}_z^{i_{a,b}} \in [\frac{1}{\gamma}\mathbf{s}_z^i, \gamma\mathbf{s}_z^i], \quad \gamma \in [1, \infty[\,. \tag{28}$$

γ is named inheritance factor. If $\gamma \neq 1$, proteins in single cells are not restricted to double during the time of one cell cycle after cell division but evolve according to the newly sampled synthesis rate. Other heterogeneous parameters can be inherited in a similar way.

Low copy numbers of molecules (such as mRNA) lead to noise after e.g. cell division. Molecules that are present in high amounts are less sensitive to stochastic variations [35]. On this basis, we assume that sister cells obtain different parameters (for example synthesis rates) but proteins which are usually present in high amounts are distributed equally to both arising cells. This is similar as described in Bertaux et al. [7] and in accordance with Spencer et al. [33]. The latter study gives a biological motivation for transient inheritance and divergence as cause of differences in synthesis rates. Spencer et al. [33] show that a correlation of sister cells exists but decreases with time after division. In the analyzed cell lines, similar responses of sister cells to induced cell death were observed up to 50 hours after cell division. This kind of information could serve as basis for fitting the value of the inheritance factor as it determines how fast correlations of sister cells are lost in the model.

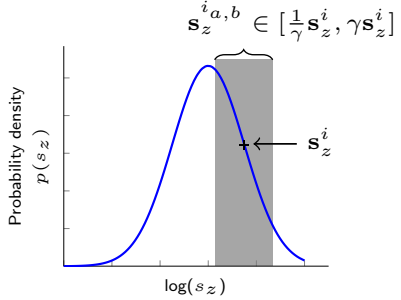

FIG. 3: **Inheritance.** The figure shows an example probability distribution of $p(s_z)$. If $\mathbf{s}_z^i$ is the sample of the protein synthesis rate in cell i, than the values $\mathbf{s}_z^{i_{a,b}}$ in corresponding daughter cells lie in the interval $[\frac{1}{\gamma}\mathbf{s}_z^i, \gamma\mathbf{s}_z^i]$.

2.4. Overall population simulation

The cell population is simulated from t_0 until t_{end}. After each cell division the dynamics of protein numbers $\dot{x}^i(t)$, (Equation (1)), and volume growth $\dot{V}^i(t)$ (Equation (3)), are simulated in the next time interval until the next division with respective new initial conditions.

At the beginning, a list called $cells$ containing all mother cells is constructed. The algorithm starts by finding the cell with the minimal simulated time and by calculating the time of this cell's next division in the case of a constant growth rate. Then, the ODE network is simulated. The simulation stops due to one of the following reasons: a) the time of the next division ($t^i_{division}$) of the cell is reached, b) t_{end}, the determined end point of the whole simulation, is reached, or c) the cell death condition is met.

If t_{end} is reached, the simulation of the cell is completed. If the cell divides, it is replaced by two daughter cells. Afterwards, it is checked whether the current number of cells exceeds the maximal possible number of cells (N_{max}). If the maximal number is exceeded, one random cell is removed from $cells$. The latter is similar to the algorithm presented by Mantzaris [26]. If the cell death condition is met, cell i is removed from $cells$. After completing the simulation of the cell, it is checked if there is another cell in the list $cells$ that is not simulated until t_{end}. Subsequently, this cell is simulated. When all cells are simulated until t_{end}, the simulation stops.

As a result, the model not only simulates the number of cells $N(t)$, but also internal distributions of parameters and proteins. A representation of the simulation algorithm is given in Figure 4. The approach is highly parallelizable, since interactions among individual cells are not modeled, and indi-

vidual cells can be simulated in parallel. The simulation algorithm is implemented in the Python toolbox `pybrn` [45].

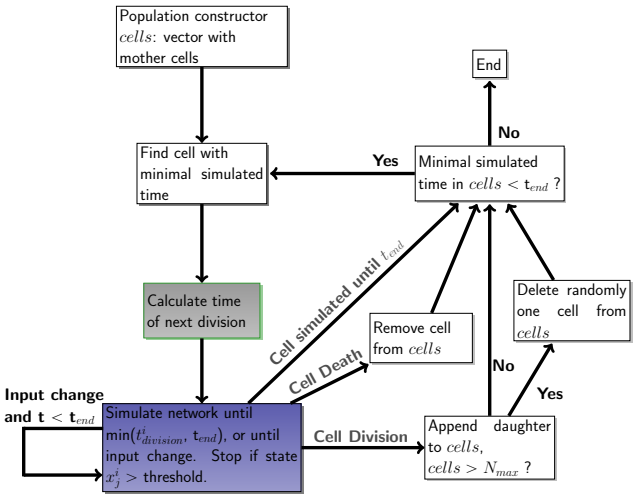

FIG. 4: **Scheme for the simulation algorithm.**

3. EXAMPLES

3.1. Example 1: Apoptotic response

Programmed cell death (apoptosis) is an important regulative process in multicellular organisms. Deregulation of apoptosis can lead to various diseases such as neurodegeneration or cancer [4, 40]. Several mathematical models of death receptor mediated apoptotic signaling pathways were published in the last decade [2, 11, 15, 20, 24, 29], a good overview is given in Spencer et al. [34]. Recently, the apoptotic response was investigated also on the level of the cell population [7, 16, 32]. TRAIL (TNF-related apoptosis-inducing ligand), an inductor of apoptosis that is interesting for medical applications in cancer treatment [44], is used exemplary. As resistance of cell populations to apoptotic stimulations is reversible [12], the example scenario is appropriate for the proposed modeling approach. The following model simulations represent *in vitro* experiments with two-dimensionally growing cancer cell populations under TRAIL stimulation. The goal of the model analyses is to gain a holistic understanding of ligand-induced effects and resistance mechanisms on the molecular and population level.

The apoptotic signaling pathway described in Eissing et al. [11] is implemented into the population modeling framework. This ODE model is a hypothetical model of a type-I cancer cell and includes main characteristics of the pathway in a simplified pattern (Figure 5). It contains eight different protein species: pro-caspase-8 (C8), activated caspase-

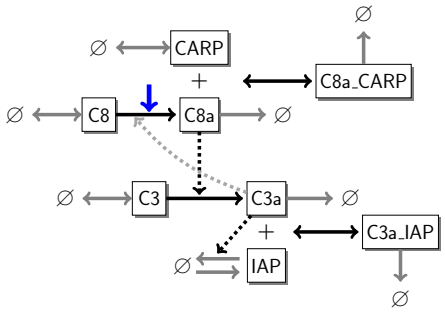

FIG. 5: **Illustration of reaction network adapted from Eissing et al. [11].** The structure of protein interactions is presented. All proteins and protein complexes are degraded. C8, C3, CARP and IAP are synthesized. C8a and C3a form complexes with CARP and IAP, respectively. C8a induces activation of C3, and C3a can induce activation of C8. C3a promotes degradation of IAP. The blue arrow indicates the TRAIL input that is added to the model.

8 (C8a), pro-caspase-3 (C3), activated caspase-3 (C3a), CARP (caspase-8- and 10-associated RING proteins), IAP (Inhibitor of Apoptosis, representing mainly XIAP), a complex of activated caspase-3 and IAP (C3a_IAP) and a complex of activated caspase-8 and CARP (C8a_CARP). Mass action kinetics are assumed. Initial conditions for the species in the single cell model of [11] are adopted as expectancy values in the population model. The protein distributions $p(X)$ are modelled as log-normal, which is biologically well supported [13]. Based on own experiments, an arithmetic coefficient of variation of about 0.65 is applied (unpublished data). With respect to the model in [11], the following major changes are implemented: First, an input u representing stimulation with the apoptosis-inducing ligand TRAIL is added (blue arrow in Figure 5). This input leads to a cleavage of pro-caspase-8. Secondly, a linear volume growth is included (Equation (3)). Thirdly, $p(s_z)$ is reconstructed with help of the deconvolution of Equation (26) and adapted so that mean and variance of $p(X_z)$ are as described. Last, the feedback from activated caspase-3 to activation of pro-caspase-8 is weakened. Reason for the latter are new biological insights that challenge the importance of the feedback [6].

Figure 6 gives an overview of the hypothetic dynamic re-

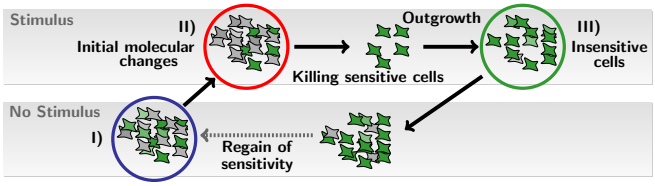

FIG. 6: **Response of a heterogeneous cell population to death receptor stimulation.** During a stimulation of a cell population with an apoptosis inducing ligand, different population structures are expected to arise. Starting with a heterogeneous cell population I), the first changes after addition of stimulus are on the molecular level, illustrated in II). Sensitive cells are killed and removed from the population and surviving cells grow out, forming a population of cells that are mainly insensitive to stimulations III). Removal of the stimulus leads to a regain of sensitivity.

sponse of a heterogeneous cell population to a stimulation with an apoptosis-inducing ligand. With help of the model, emerging population structures can be analyzed in detail.
Simulations with constant input over time were conducted and the influence of varying values of the inheritance factor γ is shown in Figure 7. According to the simulation, the inheritance factor has no influence on initially induced cell death. Instead, γ influences the outgrowth of a TRAIL-insensitive population: the higher the inheritance factor, the less resemblance from mother to daughter cells. Therefore, a higher inheritance factor increases the probability of TRAIL-sensitive daughter cells originating from an insensitive mother cell. While measuring the mean cell cycle length of a population, the inheritance factor can be adjusted to the slope of population growth trajectories in viability assays. In order to represent an intermediate inheritance, γ is set to 1.3 in the following simulations.

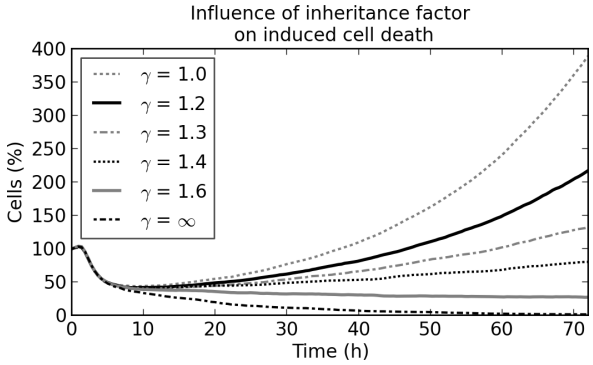

FIG. 7: **Cell population growth simulation with continuous input and varying inheritance factor.** A starting population of 5000 mother cells is simulated with constant TRAIL input over time. Simulations with different values of the inheritance factor γ were conducted and resulting population growth trajectories are plotted.

Each cell in the simulated population can be tracked in time referring to protein numbers and cell cycle stage represented by the volume. An example plot of pro-caspase-3 over time without TRAIL stimulation is shown in Figure 8. Differences in synthesis rates cause protein numbers of sister cells, originated from the same mother cell, to diverge with time. This is in accordance to Spencer et al. [33] and yields another possibility for determining the correct value of the inheritance factor from experimental data of single cell protein numbers.

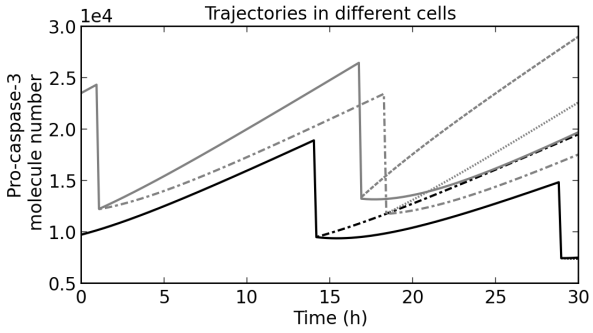

FIG. 8: **Trajectories of pro-caspase-3 molecules.** Each continuous line segment represents pro-caspase-3 numbers during a cell cycle in one cell. Discontinuities stem from cell divisions. The simulation started with two mother cells.

In order to analyze protein distributions at time points of interest during TRAIL stimulation, histogram representations are chosen. In the following, the total amount of each protein x_{tot}, including free, activated and complexed protein, is considered. Mean values for synthesis rates concern solely free and unprocessed forms.

Already 90 minutes after continuously treating a cell population with TRAIL, the model predicts the distribution of IAP_{tot} to be altered. More precisely, the distribution is elongated to the left, leading to a decreased average IAP_{tot} amount in the population (Figure 9). As synthesis rates and all other protein distributions are hardly altered at this time point (Figure 11), the decrease of IAP_{tot} is identified as main initial step towards apoptotic cell death.

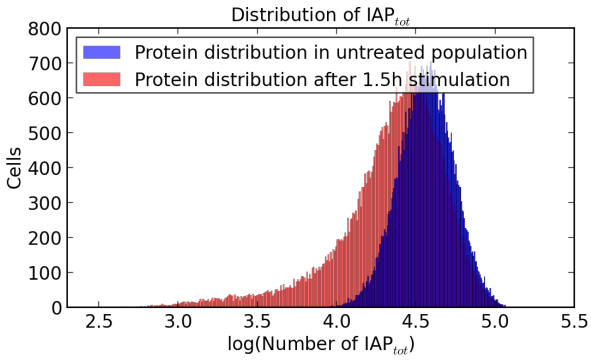

FIG. 9: **Histogram representation of total IAP distribution.** The total amount of IAP (including free IAP and the complex of IAP and activated caspase-3) in a simulated population that is treated for 90 minutes with TRAIL (red) is compared to the amount in an untreated population (blue). The number of mother cells in the starting population was 50000. Mean value in untreated population:$\sim$39600 $\frac{\text{molecules}}{\text{cell}}$ (synthesis rate IAP:$\sim$504 $\frac{\text{molecules}}{\text{min cell}}$). Mean value after 90min treatment:$\sim$28000 $\frac{\text{molecules}}{\text{cell}}$ (synthesis rate IAP:$\sim$511 $\frac{\text{molecules}}{\text{min cell}}$).

After 72h of continuous TRAIL treatment, the most significant changes are in the distribution of $C3_{tot}$ (Figure 10). Average amounts of IAP_{tot} and $CARP_{tot}$ are decreased, probably as a consequence of accelerated degradation rates of the formed protein complexes and further degradation mechanisms. Interestingly, mean synthesis rates of IAP and CARP are increased after the treatment (Figure 11). An explanation for this result is the anti-apoptotic function of both molecules, and the corresponding surviving benefit of cells with higher synthesis rates.
A 10 % variation of γ had qualitatively no influence on the results presented in Figure 11. Without stimulation, mean values for all protein amounts remain unchanged after 72h, confirming suitable initial conditions derived in Section 2 2.2.

One step towards optimization of therapeutic strategies is the simulation analysis of repeated addition of death-

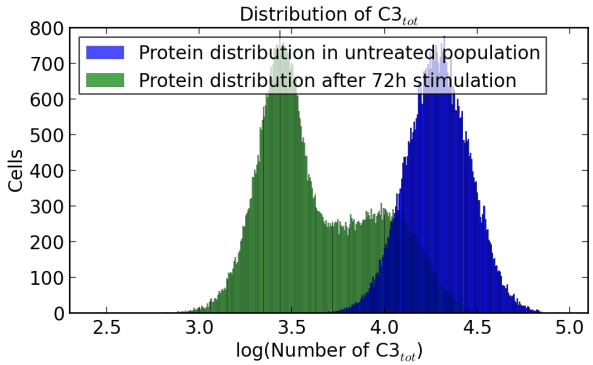

FIG. 10: **Histogram representation of total caspase-3 distribution.** The distribution of total caspase-3 in a simulated cell population after 72h continuous TRAIL treatment (green) is compared to the untreated case (blue). $C3_{tot}$ includes procaspase-3, activated caspase-3 and the complex of IAP and activated caspase-3. The number of mother cells in the starting population was 50000. Mean value in untreated population:$\sim$21100 $\frac{\text{molecules}}{\text{cell}}$ (synthesis rate C3:$\sim$103 $\frac{\text{molecules}}{\text{min cell}}$). Mean value after 72h treatment:$\sim$5800 $\frac{\text{molecules}}{\text{cell}}$ (synthesis rate C3:$\sim$71 $\frac{\text{molecules}}{\text{min cell}}$).

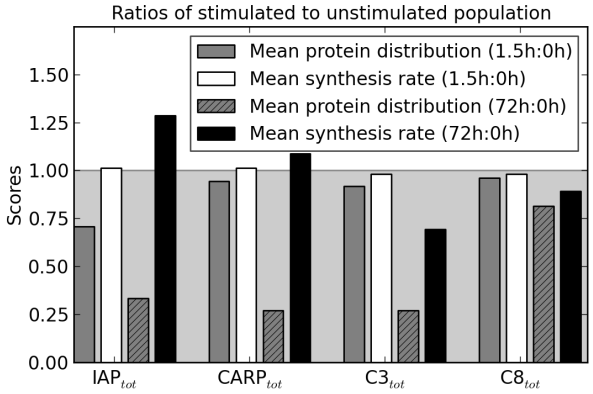

FIG. 11: **Simulation results of mean values in stimulated to unstimulated cell populations.** The mean values of simulated protein distributions and synthesis rates were divided by the respective mean values in an untreated population. Stimulation was either for 90min or for 72h, as indicated. After 90min of TRAIL treatment, the average amount of IAP$_{tot}$ per cell is decreased. Mean values of synthesis rates and all other protein distributions are hardly altered by then. After 72h of continuous TRAIL treatment, the average protein numbers per cell $C3_{tot}$, CARP$_{tot}$ and IAP$_{tot}$ are significantly decreased. Mean protein number and synthesis rate of $C8_{tot}$ are slightly lower compared to the untreated population. Treated cells exhibit increased mean values of synthesis rates of IAP and CARP. The mean synthesis rate of C3 is decreased in comparison to the untreated population.

inducing ligand to the cell population. Here, two TRAIL pulse stimulations, each for four hours, were given to the population at different time points within 72h (Figure 12). The simulation reveals the tendency that the greater the time interval between two pulses, the less cells are alive after 72h. The reason is that parameter changes upon cell division, as controlled by the inheritance factor, cause a time-dependent reversibility of TRAIL insensitivity. After the first stimulation at $t = 0$, most of the surviving cells will be insensitive to TRAIL. Daughter cells of insensitive mother cells can become TRAIL-sensitive and therefore, it is plausible that the proportion of sensitive to insensitive cells increases with time after a first stimulation. This

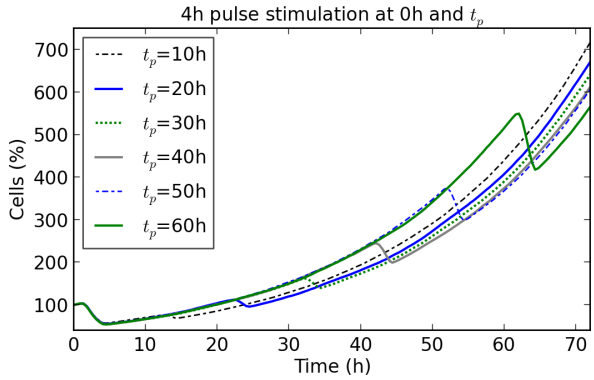

FIG. 12: **Simulations of pulse treatments at varying stimulation times.** Within 72h, two pulses of 4h each were given to a starting population of 5000 cells. The first pulse was always at $t = 0h$ and the timing of the second pulse varied from $t_p = 10h$ up to $t_p = 60h$, as indicated.

analysis can be used on the one hand for model adaption via experimental investigations and on the other hand as a starting point for an optimal treatment design.

In Table I the runtime for different simulation scenarios are illustrated. Simulations for Example 1 were performed on a 3.4 GHz Intel Core i7-4770 machine with 16 GB RAM, for Example 2 on a 1.7 GHz Intel Core i7 machine with 8 GB RAM. Number of simulated cells, inheritance factor and t_{end} were identified as main factors for varying runtimes.

TABLE I: Evaluation of runtime

	Example 1		Example 2	
# States	9	9	3	3
# Reactions	21	21	6	6
# Het. parameters	4	4	1	1
# Inheritance factor	1.3	1.3	∞	∞
# Stimulus	constant	constant	constant	pulsed
# Cells t_0	5000	50000	5000	5000
t_{end} [h]	72	1.5	100	100
# Cells alive t_{end}	6951	50659	8982	20568
# Simulated cells	37640	59444	1032	2033
# N_{max}	-	-	400	400
Runtime [min]	92.82	13.41	0.25	0.36
Figure	7	9	14	15

3.2. Example 2: Cell differentiation

As a second example, we consider a model for a differentiating cell population. The motivation for modeling this as a heterogeneous population is that there are at least two subpopulations, the progenitor cells and the differentiated

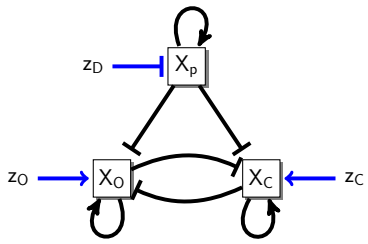

FIG. 13: **Illustration of the osteochondroswitch differentiation network. Adapted from [30].**

cells. Also, differentiation is coupled to a loss of proliferative capacity in a range of cell lineages such as myoblasts [28] or osteoblasts [5], which affects the growth dynamics of a differentiating cell population.

In addition, there is some amount of heterogeneity within each subpopulation. The major type of heterogeneity for this process is within the progenitor population: in embryonic stem cells, it has been observed that due to stochastic fluctuations in transcription factor activity, only part of the progenitor population can differentiate at any point in time, while the other part is insensitive to differentiation [21]. The study in this section aims to show that the proposed population modeling scheme can be applied to such systems, and to highlight the biological conclusions that can be drawn from the simulation of the model.

The specific single cell model on which the population model is based is taken as the "osteochondroswitch" presented in Schittler et al. [30]. The osteochondroswitch model describes the cellular state with the activities of three transcriptional regulators, as illustrated in Figure 13. Each transcriptional regulator represents one of three considered cell types: a stem cell/ progenitor type, represented by the x_p variable, an osteoblast type, represented by the x_O variable, and a chondrocyte type, represented by the x_C variable. Irreversible differentiation is modeled with a transition over a saddle-node bifurcation which is induced by a cell-type specific differentiation stimulus. In order to develop a population model as outlined in Section 2 for the osteochondroswitch, the genetic regulatory network for differentiation developed in [30] is used as a single cell model according to (1). The heterogeneity among cells is described by varying the parameter m_P, which in the original model from [30] describes the sensitivity of the cell to the differentiation stimulus: in [30], the equation for the progenitor state is given by

$$\dot{x}_P = \frac{a_P x_P^n + b_P}{m_P + z_D + c_{PP} x_P^n} - k_P x_P. \tag{29}$$

Accordingly, for a given differentiation stimulus z_D, only cells with a value of the m_P parameter larger than a threshold value, which depends on z_D, will differentiate. Using parameter values from [30] and a differentiation stimulus $z_D = 3$, the threshold for differentiation is $m_P^* \approx 7.5$. For this study, the parameter m_P is assumed to be distributed according to a log-normal distribution with a mean value of 8.0 and a standard deviation of 1.12.

Population growth is modeled with a state-dependent growth rate for individual cells, given by

$$\dot{V} = g(P), \tag{30}$$

where P is the activity of the progenitor factor in the model, which is around 12 for progenitor cells and below 1 for differentiated cells. The growth rate function $g(P)$ is modeled as a piecewise linear, ramp-like function defined as

$$g(P) = \begin{cases} 0, & P < 5 \\ g_{max}(P-5)/5, & 5 \leq P < 10 \\ g_{max}, & P \geq 10, \end{cases} \tag{31}$$

with $g_{max} = 5.56{\cdot}10^{-3}\,\mathrm{min}^{-1}$. This choice of $g(P)$ means that in the model, progenitor cells grow with a cell cycle duration of 30 h, and differentiated cells do not grow. The inheritance factor defined in (28) is set to infinity, meaning that the heterogeneous parameter is resampled from the original distribution upon each cell division. Two scenarios for a population of osteochondroswitches were simulated, starting from a population where all cells are in the progenitor state.

In the first scenario, a constant differentiation stimulus ($z_D = 3$ in the nomenclature of [30]) and osteoblast specific stimulus ($z_O = 0.5$ in the nomenclature of [30]) were applied. Figure 14 displays the results of the population simulation for the first scenario. At the beginning, many progenitor cells differentiate to osteoblasts. The progenitor cells that are not sensitive to differentiation at the beginning divide, but upon division may become sensitive and, since the stimulus is applied continuously, differentiate. Thus, there is a small continuous growth of the osteoblast subpopulation, and a slowly declining progenitor population. The simulation results also show a shift in the distribution for the differentiation sensitivity parameter over time: as cells with a high parameter value differentiate to osteoblasts and make up for an increasing fraction of the population, the density of high values increases compared to the density of low values.

In the second scenario, the same stimulus was applied in two pulses, one at time zero and the other at time 50 h, with a duration of 10 h for each pulse. The simulation results for this scenario are shown in Figure 15. The pulse stimulation results in very different growth dynamics compared to the first scenario. While the number of cells differentiating during the first 10 h is about the same, the progenitor population is quickly growing back to its original size when the differentiation pulse ceases. Upon the second pulse, again a large proportion of the regrown progenitor population differentiates to osteoblasts. At the end of the considered time interval, the numbers of both total and differentiated cells are significantly higher than in the first scenario. Regarding

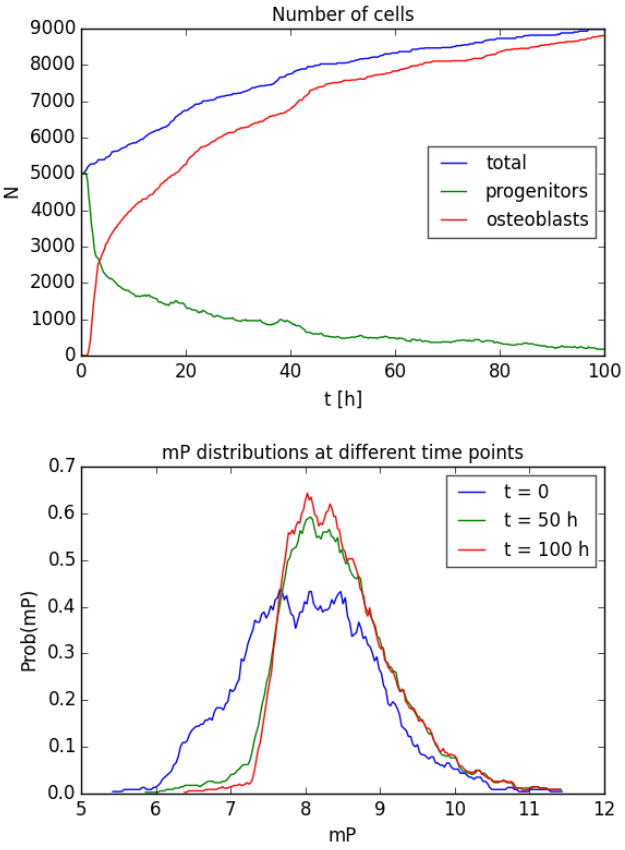

FIG. 14: **Osteochondroswitch population under a continuous differentiation stimulus.** Top panel: Population sizes over time. Bottom panel: Population heterogeneity in the sensitivity parameter m_P at three time points.

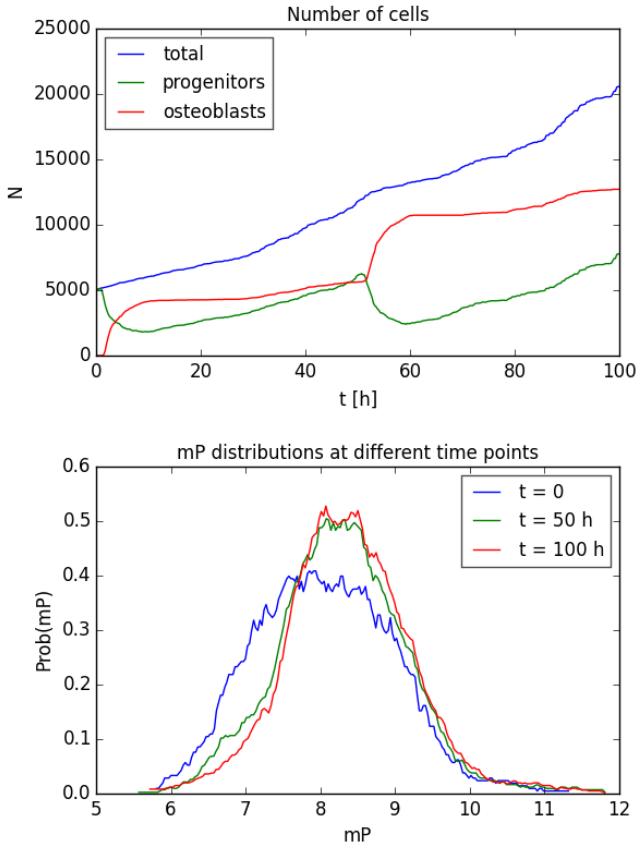

FIG. 15: **Osteochondroswitch population with two differentiation pulses.** Top panel: Population sizes over time. Bottom panel: Population heterogeneity in the sensitivity parameter m_P at three time points.

the distribution of the sensitivity parameter, a similar development as in the first scenario is observed. However, the density at low values is still higher at the later time points, due to the regrown progenitor population.

4. CONCLUSIONS

A sample-based ODE approach describing a heterogeneous cell population during extrinsic stimulations is developed. In contrast to previously published models, the presented individual-based population model connects intracellular reaction networks with cell division, cell death and inheritance, while stochastic effects are solely considered in initial conditions and by resampling of parameters after cell division. Appropriate initial conditions for unstimulated stationary growing populations are derived and an inheritance factor that determines the degree of similarites between parameters in mother and daughter cells is introduced.

The first application to induced cell death shows that the model helps to understand resistance mechanisms of cancer cells during drug treatment. Long-term goals are an optimization of drug efficiency and the improvement of anticancer strategies. In the example, the underlying inheritance factor can be estimated with help of the following information: a) Measurement of cell population growth over time during continuous TRAIL stimulation and evaluation of the slope of cell growth trajectories after initial cell death. b) Measurement of similarity between mother and daughter cells. c) Pulse stimulations and evaluation of the influence of the second pulse. With help of the model, different hypotheses referring to the apoptotic response of a heterogeneous cell population can be stated. First, the distribution in the total amount of IAP is initially shifted after drug induction. Hence, IAP is important for the first molecular changes in a cell population that lead to apoptotic cell death. Secondly, considering a treatment of 72h, the model predicts a clear decrease of mean values in all protein distributions except of the total amount of caspase-8. As a conclusion, the role of caspase-8 in TRAIL insensitivity of a type-I cell population can be challenged. Synthesis rates of CARP and IAP are predicted to be increased after 72h treatment, illustrating survival benefit because of the anti-apoptotic effects of these molecules. Thirdly, a simulation of a pulse treatment revealed that if two pulses of a fixed

duration are given to a population, a large time interval between those pulses is preferable in order to kill the maximal number of the cells. Predictions are limited to the included model of simplified type-I extrinsic apoptosis [11]. Other apoptotic models can be included into the framework and can be analyzed in a similar way.

The second example with the differentiating cell population illustrates the usefulness of the developed population simulation framework for populations with distinct subpopulations. A particular aspect is the differential growth dynamics among the subpopulations, which gave rise to different growth dynamics for different temporal shapes of the differentiation stimulus. The model may be useful in tissue engineering applications, where the design of the external stimulus to optimize tissue generation is one of the key issues.

In conclusion, the population simulation framework developed in this paper is an effective and versatile tool for the computational analysis of dynamic, heterogeneous cell populations on multiple scales. It is applicable to a wide range of biological systems and intracellular processes, including gene regulation and biochemical signal transduction.

5. ACKNOWLEDGMENTS

The authors acknowledge funding from the German Federal Research and Education Ministry (BMBF) in the project "PREDICT", and from the German research foundation in the grant SCHE 349/10-1. Furthermore, we thank Jun.-Prof. Thomas Kahle and Karsten Kuritz for fruitful discussions and Caterina Thomaseth for comments on preliminary versions.

References

[1] N. Aghaeepour, R. Nikolic, H. H. Hoos, R. R. Brinkman. Rapid cell population identification in flow cytometry data. *Cytometry. Part A : Journal of the International Society for Advancement of Cytology*, 79(1):6-13, **(2011)**

[2] J. G. Albeck, J. M. Burke, B. B. Aldridge, M. Zhang, D. A. Lauffenburger, P. K. Sorger. Quantitative analysis of pathways controlling extrinsic apoptosis in single cells. *Molecular Cell*, 30(1):11-25, **(2008)**

[3] V. Andasari, A. Gerisch, G. Lolas, A. P. South, M. A. J. Chaplain. Mathematical modeling of cancer cell invasion of tissue: biological insight from mathematical analysis and computational simulation. *Journal of Mathematical Biology*, 63(1):141-171, **(2011)**

[4] A. Ashkenazi and V. M. Dixit. Death receptors: signaling and modulation. *Science*, 281(5381):1305-1308, **(1998)**

[5] J. E. Aubin, F. Liu, L. Malaval, A. K. Gupta. Osteoblast and chondroblast differentiation. *Bone*, 17(2-Suppl.1):S77–S83, **(1995)**

[6] J. Beaudouin, C. Liesche, S. Aschenbrenner, M. Hörner, R. Eils. Caspase-8 cleaves its substrates from the plasma membrane upon CD95-induced apoptosis. *Cell Death and Differentiation*, 20(4):599-610, **(2013)**

[7] F. Bertaux, S. Stoma, D. Drasdo, G. Batt. Modeling dynamics of cell-to-cell variability in TRAIL-induced apoptosis explains fractional killing and predicts reversible resistance. *PLOS Computational Biology*, 10(10): e1003893. doi:10.1371/journal.pcbi.1003893, **(2014)**

[8] I. Conlon, M. Raff. Differences in the way a mammalian cell and yeast cells coordinate cell growth and cell-cycle progression. *Journal of Biology*, 2(7), doi:10.1186/1475-4924-2-7 **(2003)**

[9] S. Cooper. Distinguishing between linear and exponential cell growth during the division cycle: Single-cell studies, cell-culture studies, and the object of cell-cycle research. *Theoretical Biology and Medical Modelling*, 3(10), doi:10.1186/1742-4682-3-10 **(2006)**

[10] M. M. Domach, M. L. Shuler. A finite representation model for an asynchronous culture of *E. coli*. *Biotechnology and Bioengineering*, XXVI:877-884, **(1984)**

[11] T. Eissing, H. Conzelmann, E. D. Gilles, F. Allgöwer, E. Bullinger, P. Scheurich. Bistability analyses of a caspase activation model for receptor-induced apoptosis. *Journal of Biological Chemistry*, 279(35):36892-36897, **(2004)**

[12] D. A. Flusberg, J. Roux, S. L. Spencer, P. K. Sorger. Cells surviving fractional killing by TRAIL exhibit transient but sustainable resistance and inflammatory phenotypes. *Molecular Biology of the Cell*, 24(14):2186-2200, **(2013)**

[13] C. Furusawa, T. Suzuki, A. Kashiwagi, T. Yomo, K. Kaneko. Ubiquity of log-normal distributions in intra-cellular reaction dynamics. *Biophysics*, 1:25-31, **(2005)**

[14] S. Gaudet, S. L. Spencer, W. W. Chen, P. K. Sorger. Exploring the contextual sensitivity of factors that determine cell-to-cell variability in receptor-mediated apoptosis. *PLOS Computational Biology*, 8(4): e1002482, **(2012)**

[15] H. A. Harrington, K. L. Ho, S. Ghosh, K. C. Tung. Construction and analysis of a modular model of caspase activation in apoptosis. *Theoretical Biology and Medical Modelling*, 5:26, doi:10.1186/1742-4682-5-26, **(2008)**

[16] J. Hasenauer, J. Heinrich, M. Doszczak, P. Scheurich, D. Weiskopf, F. Allgöwer. Visualization methods and support vector machines as tools for determining markers in models of heterogeneous populations: Proapoptotic signaling as a case study. *Proceedings of Eigth International Workshop on Computational Systems Biology (WCSB 2011)*, p.61–64, **(2011)**, Zurich, Switzerland

[17] J. Hasenauer, S. Waldherr, M. Doszczak, P. Scheurich, N. Radde, F. Allgöwer. Analysis of heterogeneous cell populations: A density-based modeling and identification framework. *Journal of Process Control*, 21(10):1417–1425, **(2011)**

[18] J. Hasenauer, S. Waldherr, N. Radde, M. Doszczak, P. Scheurich, F. Allgöwer. A maximum likelihood estimator for parameter distributions in heterogeneous cell populations. *Procedia Computer Science*, 1(1):1655-1663, **(2010)**

[19] M. A. Henson, D. Müller, M. Reuss. Cell population modelling of yeast glycolytic oscillations. *Biochemical Journal*, 368:433–446, **(2002)**

[20] S. M. Kallenberger, J. Beaudouin, J. Claus, C. Fischer, P. K. Sorger, S. Legewie, R. Eils. Intra- and interdimeric caspase-8 self-cleavage controls strength and timing of CD95-induced apoptosis. *Science signaling*, 7(316):ra23, **(2014)**

[21] T. Kalmar, C. Lim, P. Hayward, S. Muñoz-Descalzo, J. Nichols, J. Garcia-Ojalvo, A. M. Arias. Regulated fluctuations in nanog expression mediate cell fate decisions in embryonic stem cells. *PLoS Biol*, 7(7):e1000149, **(2009)**

[22] H. E. Kubitschek. Normal distribution of cell generation rates. *Nature*, 209(5027):1039–1040, **(1966)**

[23] H. E. Kubitschek. Evidence for the generality of linear cell growth. *Journal of Theoretical Biology*, 28(1):15-29, **(1970)**

[24] S. Legewie, N. Blüthgen, H. Herzel. Mathematical modeling identifies inhibitors of apoptosis as mediators of positive feedback and bistability. *PLOS Computational Biology*, 2(9):1061–1073, **(2006)**

[25] M. E. Lidstrom, and M. C. Konopka. The role of physiological heterogeneity in microbial population behavior. *Nature Chemical Biology*, 6(10):705–712, **(2010)**

[26] N. V. Mantzaris. Stochastic and deterministic simulations of heterogeneous cell population dynamics. *Journal of Theoretical Biology*, 241:690–706, **(2006)**

[27] H. H. McAdams, A. Arkin. It's a noisy business! Genetic regulation at the nanomolar scale. *Trends in genetics*, 15(2):65-69, **(1999)**

[28] B. Nadal-Ginard. Commitment, fusion and biochemical differentiation of a myogenic cell line in the absence of dna synthesis. *Cell*, 15(3):855–864, **(1978)**

[29] M. Rehm, H. J. Huber, H. Dussmann, J. H. M. Prehn. Systems analysis of effector caspase activation and its control by X-linked inhibitor of apoptosis protein. *The EMBO Journal*, 25(18):4338-4349, **(2006)**

[30] D. Schittler, J. Hasenauer, F. Allgöwer, S. Waldherr. Cell differentiation modeled via a coupled two-switch regulatory network. *Chaos*, 20(4):045121, doi:10.1063/1.3505000, **(2010)**

[31] D. Schittler, J. Hasenauer, F. Allgöwer. A generalized population model for cell proliferation: Integrating division numbers and label dynamics. *Proceedings of Eigth International Workshop on Computational Systems Biology (WCSB 2011)*, p. 165–168 **(2011)** June, Zurich, Switzerland

[32] M. Schliemann, E. Bullinger, S. Borchers, F. Allgöwer, R. Findeisen, P. Scheurich. Heterogeneity reduces sensitivity of cell death for TNF-Stimuli. *BMC Systems Biology*, 5:204, doi:10.1186/1752-0509-5-204, **(2011)**

[33] S. L. Spencer, S. Gaudet, J. G. Albeck, J. M. Burke, P. K. Sorger. Non-genetic origins of cell-to-cell variability in TRAIL-induced apoptosis. *Nature*, 459(7245):428-432, **(2009)**

[34] S. L. Spencer, P. K. Sorger. Measuring and modeling apoptosis in single cells. *Cell*, 144(6):926–939, **(2011)**

[35] J. L. Spudich, J. D. E. Koshland Jr. Non-genetic individuality: chance in the single cell. *Nature*, 262:467–471, **(1976)**

[36] T. M. Squires, R. J. Messinger, S. R. Manalis. Making it stick: convection, reaction and diffusion in surface-based biosensors. *Nature biotechnology*, 26(4):417–426, **(2008)**

[37] M. Stamatakis, K. Zygourakis. A mathematical and computational approach for integrating the major sources of cell population heterogeneity. *Journal of Theoretical Biology*, 266:41–61, **(2010)**

[38] P. S. Swain, M. B. Elowitz, E. D. Siggia. Intrinsic and extrinsic contributions to stochasticity in gene expression. *PNAS,*, 99(20):12795–12800, **(2002)**

[39] S. C. Taylor, T. Berkelman, G. Yadav, M. Hammond. A defined methodology for reliable quantification of Western blot data. *Molecular Biotechnology*, 55(3):217-226, **(2013)**

[40] N. A. Thornberry, Y. Lazebnik. Caspases: enemies within. *Science*, 281(5381):1312-1316, **(1998)**

[41] A. Tzur, R. Kafri, V. S. LeBleu, G. Lahav, M. W. Kirschner. Cell growth and size homeostasis in proliferating animal cells. *Science*, 325(5937):167-171, **(2009)**

[42] D. Volfson, J. Marciniak, W. J. Blake, N. Ostroff, L. S. Tsimring, J. Hasty. Origins of extrinsic variability in eukaryotic gene expression. *Nature*, 439(7078):861-864, **(2006)**

[43] S. Waldherr, J. Hasenauer, F. Allgöwer. Estimation of biochemical network parameter distributions in cell populations. *Proceedings of the 15th IFAC Symposium on System Identification (SYSID)*, p. 1265–1270, **(2009)** September 27, Saint-Malo, France

[44] S. R. Wiley, K. Schooley, P. J. Smolak, W. S. Din, C. Huang, J. K. Nicholl, G. R. Sutherland, T. D. Smith, C. Rauch, C. A. Smith, R. G. Goodwin. Identification and characterization of a new member of the TNF family that induces apoptosis. *Immunity*, 3(6):673–682, **(1995)**

[45] http://pybrn.sourceforge.net